AGU PUBLICATIONS

JGR

Journal of Geophysical Research: Oceans

RESEARCH ARTICLE

10.1002/2016JC011777

Evidence of rising and poleward shift of storm surge in western North Pacific in recent decades

Lie-Yauw Oey[1,2] and Simon Chou[1]

[1]Graduate Institute of Hydrological & Oceanic Sciences, National Central University, Taoyuan, Taiwan, [2]Program in Atmospheric & Oceanic Sciences, Princeton University, Princeton, New Jersey, USA

Key Points:
- Storm surge can potentially become more intense and variable as the climate warms
- We give evidence of rising and poleward shift of storm surge in western North Pacific
- We relate the rising and poleward-shifting surges to recurving and slower typhoons caused by weakening steering flow due to climate change

Supporting Information:
- Supporting Information S1

Correspondence to:
L. Oey,
lyooey@gmail.com

Citation:
Oey, L-Y., and S. Chou (2016), Evidence of rising and poleward shift of storm surge in western North Pacific in recent decades, *J. Geophys. Res. Oceans*, *121*, 5181–5192, doi:10.1002/2016JC011777.

Received 5 MAR 2016
Accepted 10 JUN 2016
Accepted article online 14 JUN 2016
Published online 30 JUL 2016

Abstract Recently, there has been considerable interest in examining how sea-level extremes due to storm surge may be related to climate change. Evidence of how storm-surge extremes have evolved since the start of the most recent warming of mid-1970s and early 1980s has not been firmly established however. Here we use 64 years (1950–2013) of observations and model simulations, and find evidence of a significant rise in the intensity as well as poleward-shifting of location of typhoon surges in the western North Pacific after 1980s. The rising and poleward-shifting trends are caused by the weakening of the steering flow in the tropics, which is related to climate warming, resulting in slower-moving and longer-lasting typhoons which had shifted northward.

1. Introduction

Approximately 60% of all tropical cyclones (TCs; or typhoons) that originate over the warm pool of the western North Pacific Ocean traverse west and northwestward across 130E (Fig. 1a), and nearly all of them make landfalls, causing considerable economic losses and human sufferings to the affected coastal regions [*Elsner and Liu*, 2003]. According to the International Best Track Archive for Climate Stewardship (IBTrACS) data [*Knapp et al*., 2010], an average of 5–6 typhoon landings per year from 1950 to 2013 was recorded along East Asia (Figure 1a). Here, approximately 73 million people live within the 1 m coastal flood plain [*Han et al*.,1995], thousands had perished since the 1950s and economic losses ran in billions of US$, making the region a high destructive potential for storm surges [*Peduzzi et al*., 2012; *Aon Benfield*, 2013; *Needham et al*., 2015].

As the climate warms, some studies have predicted an increase in the global mean of TC intensity, while the frequency decreases [*Bender et al*., 2010; *Knutson et al*., 2010, 2013, 2015]. Another study predicts increases both in the TC intensity and frequency, which are significant in the western North Pacific [*Emanuel*, 2013]. A recent review is *Walsh et al* [2015]. Studies using historical data report imprints of climate warming on TCs, showing significant changes especially since the late 1970s and early 1980s [e.g., *Emanuel*, 2005; *Kossin et al*., 2014], coincident with the start of the rapid rise in global SST [*Rayner et al*., 2006; *Trenberth et al*., 2007; *Hansen et al*., 2010; *Balmaseda et al*., 2013]. Together with sea-level rise [*Levermann et al*., 2005; *Yin et al*., 2009; *Goddard et al*., 2015], which exacerbates risks to coastal populations due to potentially more frequent inundations [*IPCC*, 2013], there is considerable interest in relating trends of TC characteristics to storm surge. Future projections using models have been conducted [*Lin et al*., 2012; *Grinsted et al*., 2013], while other studies have examined changes in storm surge extremes analyzed from tide gauge data with large-scale indices such as the PDO and NAO [*Feng and Tsimplis*, 2014; *Marcos et al*., 2015]. *Grinsted et al*. [2012, 2013] found using a statistical model teleconnection between SST and Atlantic hurricane surges: e.g., ENSO and Atlantic hurricanes [*Gray* 1984; *Elsner and Liu*, 2003]. *Bromirski and Kossin* [2008] found that waves along the U.S. east coast and Gulf of Mexico are closely related to North Atlantic hurricane activity. On the other hand, a direct link between storm surge in the western North Pacific and climate warming that has undergone since the 1970s–1980s has not been made.

The East Asian Pacific rim has also experienced a significant sea-level rise in the past 3 decades [*Merrifield*, 2011]. Although storm surge simulations have been conducted for anecdotal events [*Chen and Qin*, 1985; *Li et al*., 2009; *Aschariyapotha et al*., 2011; *Lin et al*., 2013; *Deng et al*., 2014; *Ding and Ding*, 2014; *Mori et al*., 2014], there is no account of the impacts on storm surge of long-term changes in TC characteristics, while observational analysis of sea-level extremes suggests a potentially strong connection between them [*Feng and Tsimplis*, 2014]. This study analyses tide gauge observations along the East Asian continent, and

simulates storm surges forced by observed TC track and intensity data from 1950–2013. We focus on the contiguous coastline of China stretching some 3000 km from south to north where relatively long-term data are available. Along a contiguous coastline, strong surges more readily develop due to forced and free coastally trapped waves [*Gill*, 1982], and trends of their intensity and locations can be more easily estimated. We found a significant rise in intensity and northward shift of the location of storm surge, which can be attributed to generally slower-moving and longer-lasting storms that also have shifted northward [*Chu et al.*, 2012; *Kossin et al.*, 2014]. The trends become significant after 1982, following a rapid increase in the global SST which began in the mid-1970s [*Nitta and Yamada*, 1989; *Trenberth*, 1990].

2. Method

2.1. A Storm Surge Model

To simulate storm surges, the parallelized version of the Princeton Ocean Model [*Mellor*, 2004], the mpiPOM [*Oey et al.*, 2013, 2014], was used over the domain 12°S–42°N and 99°E–130°E at a resolution of 0.05° × 0.05°, including the East Asian continent (but excluding Japan). Model terrain (ocean depths and land heights) was interpolated from the 2 min ETOPO2 data (http://www.ngdc.noaa.gov/mgg/fliers/01mgg04.html), and the inundation scheme was based on *Oey* [2005, 2006]. The model solves the following depth-averaged equations:

$$\partial\eta/\partial t+\nabla.(\boldsymbol{u}D) \;=\; 0 \tag{1a}$$

$$\partial(D\boldsymbol{u})/\partial t+\partial(uD\mathbf{u})/\partial x+\partial(vD\boldsymbol{u})/\partial y+\boldsymbol{k}Df\times\boldsymbol{u}= \;-Dg\nabla(\eta-\eta_a-\eta_{eq}) \;+\tau^o-\tau_b, \tag{1b,1c}$$

which assume that the water density (ρ) is constant and fluid is incompressible. Here η is sea-surface height (SSH) referenced to the mean sea level (MSL), t is time, $\nabla=(\partial/\partial x,\partial/\partial y)$ is the horizontal gradient operator, $\boldsymbol{x}=(x, y)$ is horizontal coordinate (x = zonal and y = meridional), $\boldsymbol{u}=(u, v)$ is the depth-averaged horizontal velocity, $D=H+\eta$ is total water depth, H = undisturbed water depth below MSL, $\boldsymbol{k}$ is vertical unit vector, $f=2\Omega.\sin(\theta)$ the Coriolis parameter, $\Omega=7.292\times10^{-5}$ s^{-1}, θ is latitude, $g=9.801$ m s^{-2}, $\eta_a(\boldsymbol{x}, t)=(p_{am}-p_a)/(\rho_o g)$ is SSH induced by atmospheric sea-level pressure (SLP) $p_a(\boldsymbol{x},t)$, p_{am} is mean SLP taken to be 1.012×10^6 N m^{-2}, η_{eq} is ($g^{-1}\times$) tidal potential accounting for all but the three shallow-water tides (M4, MS4, and MN4), $=\Sigma_n\eta_n$, i.e., consisting of the sum of 22 equilibrium tidal constituents η_n's which depend on the Love numbers and potential amplitudes (as well as on longitude and latitude) [*Cartwright*, 1978], and τ^o and τ_b are kinematic wind stress and bottom stress vectors, respectively. The kinematic bottom stress is:

$$\tau_b=gn^2|\boldsymbol{u}|\boldsymbol{u}.D^{-1/3} \tag{2}$$

where the Manning's coefficient n is set = 0.03 m$^{-1/3}$ s [e.g., *Chow*, 1959]. Contributions from the tidal potential (η_{eq}) are included to improve accuracy [*Sauvaget et al.*, 2000]. Tides are specified along the open boundaries [*Oey et al.*, 1985; *Lefevre et al.*, 2000] together with radiation condition to reduce the reflections of interior disturbances (due e.g., to storms) back into the modeled domain [*Oey and Chen*, 1992; *Cummins and Oey*, 1997]. Eight dominant tidal constituents (M2, S2, K1, O1, N2, K2, P1, Q1) are used. The modeled tides have been extensively validated against tide-gauge data obtained from the University of Hawaii Sea Level Center [http://ilikai.soest.hawaii.edu/uhslc/data.html] and the model is being used for real-time forecasting [http://mpipom.ihs.ncu.edu.tw/showForecasts/tide.php].

2.2. TC Winds

Three analysis products of 6 hourly wind are used to drive the model: (i) National Center for Environmental Prediction (NCEP; 1/2° × 1/2° grid) from 1950 to 2013, (ii) European Center for Medium Range Weather Forecast (ECMWF; 3/4° × 3/4° grid) from 1962 to 2013, and (iii) cross-calibrated multi-platform wind (CCMP, 1/4° × 1/4° grid) from 1988 to 2013. Because of their coarse resolutions, these winds underestimate the maximum wind speeds by as much as 50%. A TC wind for each storm is therefore calculated using the *Holland* [1980] vortex model with parameters from the IBTrACS observational data set [*Knapp et al.*, 2010], which includes TC maximum wind speeds, minimum SLP, and center locations; the radius of maximum wind is unavailable and is assumed to be 30 km [*Sun and Oey*, 2015]. These variables from different TC Centers (e.g., CMA, HKO, JMA, JTWC) in the IBTrACS data set are ensemble-averaged to form a complete, gapless data set, which for simplicity will be referred to as the IBTrACS. The Holland vortex wind is then used to embed and merge TCs into each of the three analysis winds using a Gaussian weight with e^{-1}-decay radius

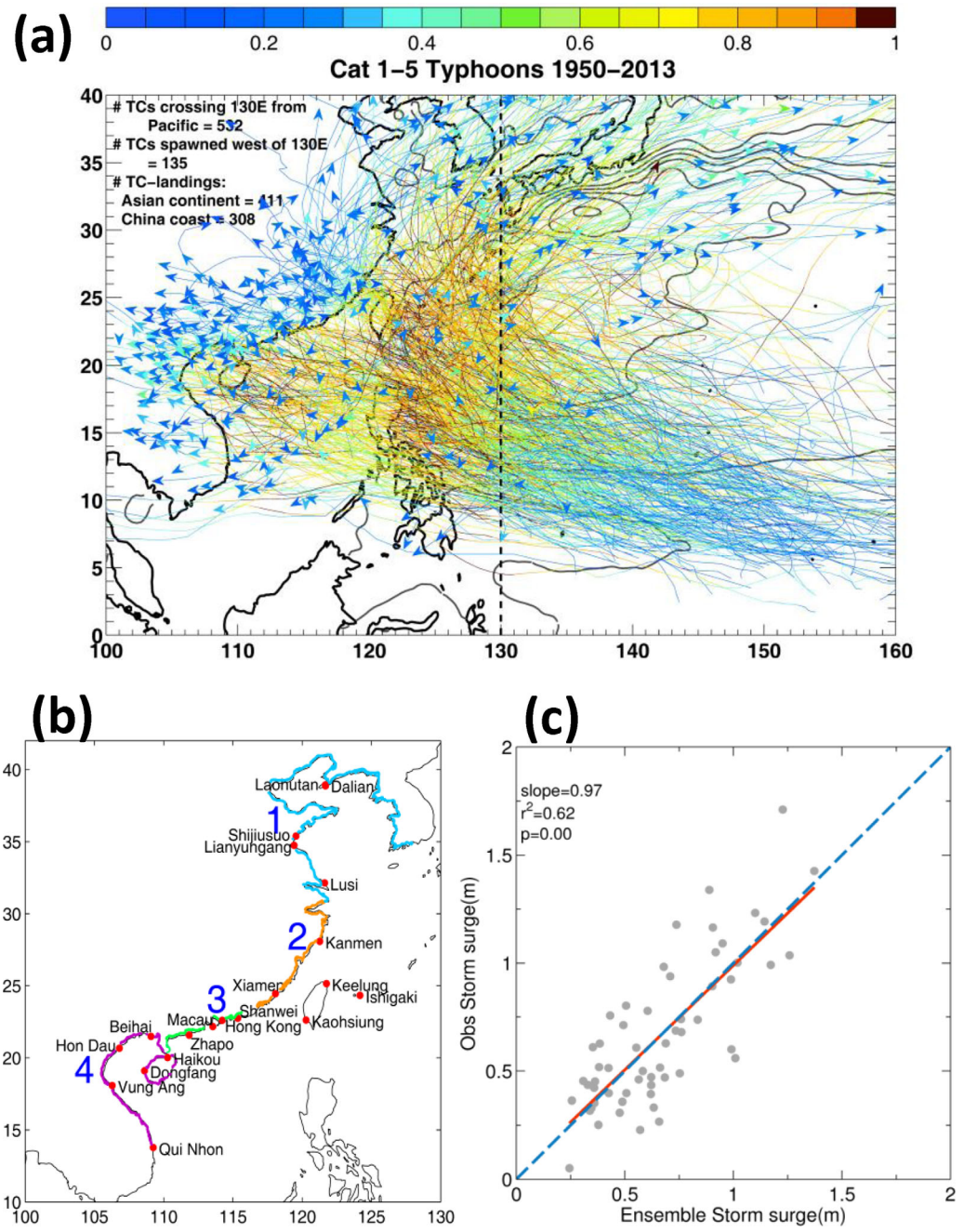

Figure 1. (a) Tracks for period 1950–2013 from the IBTrACS observations of typhoons (maximum sustained wind speeds > 33 m s^{-1}) which crossed westward across 130°E. Color on each track indicates the observed 6 hourly wind speed normalized by the maximum wind speed for that track. Total number of typhoons in the whole region was 667 (532 + 135), of which 411 made landfalls on the Asian continent including 308 over China, and the remainder (256) either recurved into the open Pacific or died before landfall. Thick contours show mean absolute dynamic topography (*m*) from AVISO (http://www.aviso.oceanobs. com/) indicating the Kuroshio and the subtropical gyre. (b) Tide-gauge locations from the University of Hawaii sea-level data center (http://uhslc.soest.hawaii.edu/) and along-coast sections 1, 2, 3, and 4 (colored) referred to in the text. (c) Comparison of observed (ordinate) and model ensemble (abscissa) storm surges from 1988 to 2013. Legends show the slope and r^2 and *p*-values of the regression line. Model ensemble is an arithmetic average of simulated storm surges using four different winds: Holland wind, CCMP + Holland wind, NCEP + Holland wind, and ECMWF + Holland wind (see Method). The period from 1988 to 2013 is chosen as it is the longest period during which the four winds overlap.

of 350 km, such that the weak TCs in the latter are replaced by the IBTrACS TCs but there is a smooth transition from Holland to analysis wind at distances far from the TC center [*Sun et al.*, 2015]. The merged wind velocity is linearly interpolated at each time step to calculate the corresponding wind stress using the *Oey*

et al.'s [2007] wind-drag formula with high wind-speed limit [*Powell et al.*, 2003]. For each wind input, integrations are carried out for the typhoon season from June through November of each year, from 1950 to 2013. An experiment driven by the Holland wind only is also conducted. These experiments with wind and tides give the sea surface height as η. Finally, another run driven by tides only yields η_T, and storm surge (η_S) is defined as their difference:

$$\eta_S = \eta - \eta_T. \tag{3}$$

2.3. Comparison of Observed and Modeled Storm Surges

We validate the model by comparing simulated and observed storm surges at tide-gauge stations (Figure 1b). Observed storm surge is calculated by removing tides extracted from the observation using the method of *Pawlowicz et al.* [2002]. Ensemble (arithmetic) averages of the modeled storm surges using the four different wind products are compared with observed storm surges for the period 1988–2013 during which the four wind products overlap (Figure 1c). The agreements between modeled and observed storm surges are satisfactory with $r^2 = 0.62$ and slope of regression line = 0.97.

3. Results

Typhoon frequency $f_{tc}(\boldsymbol{x})$ over the Philippines and Taiwan coasts shows on average more than 0.5 day per season (June–November) of typhoon-strength winds (Figure 2a). Central and southern China coastlines experience more than 1 h per season, and north of 30°N in the Yellow Sea along the coastlines of northeastern China and Korea typhoon-strength winds are less than 1 h per season. The strong winds penetrate 100–200 km inland of nearly all of the coastline of China (Figure 2a); however, and as a storm approaches the coast and makes landfall, coastal-trapped waves [*Gill*, 1982] are produced and reinforced as the waves propagate along the long and relatively smooth coastline of China, exciting surges at more distant locations. Thus despite the comparatively low f_{tc} along the China coast, the maximum storm surge $\eta_{Smax}(\boldsymbol{x})$ ($= \mathrm{Max}|_t(\eta_S)$, where t is time and storm surge η_S is defined as total sea level minus tides), often exceeds 1 m (Figure 2a red shading and white contours), while strong surges around islands (e.g., Taiwan) are weaker. On average for the past 64 years (1950–2013), there were more than 2 storm surges per season with sea level exceeding 0.7 m (Figure 2b left) and at least 1 per season exceeding 1 m (Figure 2b right) along the coast of China.

3.1. Simulated Storm Surge Trends

Monthly maximum model storm surges $\eta_{Smax}(\boldsymbol{x})$ and the corresponding latitudes θ_{Smax} were averaged over each season to form 64 seasonally mean maxima $<\eta_{Smax}>$ and $<\theta_{Smax}>$ from 1950 to 2013, and then ensemble-averaged over the four wind cases. The $<\eta_{Smax}>$ shows an increasing trend of 0.06 m per decade over the whole analysis period from 1950 to 2013, significant at the 98% confidence level (Figure 3a). There is not a significant trend for the first half of the record from 1950 to 1981, but a strong rising trend of 0.14 m per decade for the second half from 1982 to 2013, significant at the 93% confidence level. These trends compare well with trends of the 99.9th centile of sea level observations from tide gauge reported by *Feng and Tsimplis* [2014], which range from 0.02 to 0.14 with a mean of 0.06 m per decade. They also compare well with the corresponding maximum storm surge trends computed at each tide gauge station, which give a mean trend of 0.07 with a range 0.03–0.17 m per decade (below; supporting information Figures S1–S2 and Table S2).

During the second period, the $<\theta_{Smax}>$ also shows a poleward shift of 0.92 degree latitude per decade, significant at the 90% confidence level (Figure 3b); neither the whole record (1950–2013) nor the first half (1950–1981) shows a significant poleward shifting trend. These results of lack of significant trends during the earlier period from 1950 to 1981, but rising trends of storm surge amplitude and poleward shifting of its location during the most recent decades from 1982 to 2013 are robust, and exist also for the individual experiments using the four different winds (supporting information Table S1). The poleward shift of storm surge leads to an increased trend in the "surge density," defined as $t_{SS>\eta 0}$ = number of hours per coastal length L (= 100 km) when the storm surge (SS) is higher than η_0. For $\eta_0 = 0.7$ m, which is near the 99th centile of the surge, the $<t_{SS>0.7m}>$ has a significant increasing trend of 1.7 h/100 km per decade (Figure 3c) for the coastline from southern to central China.

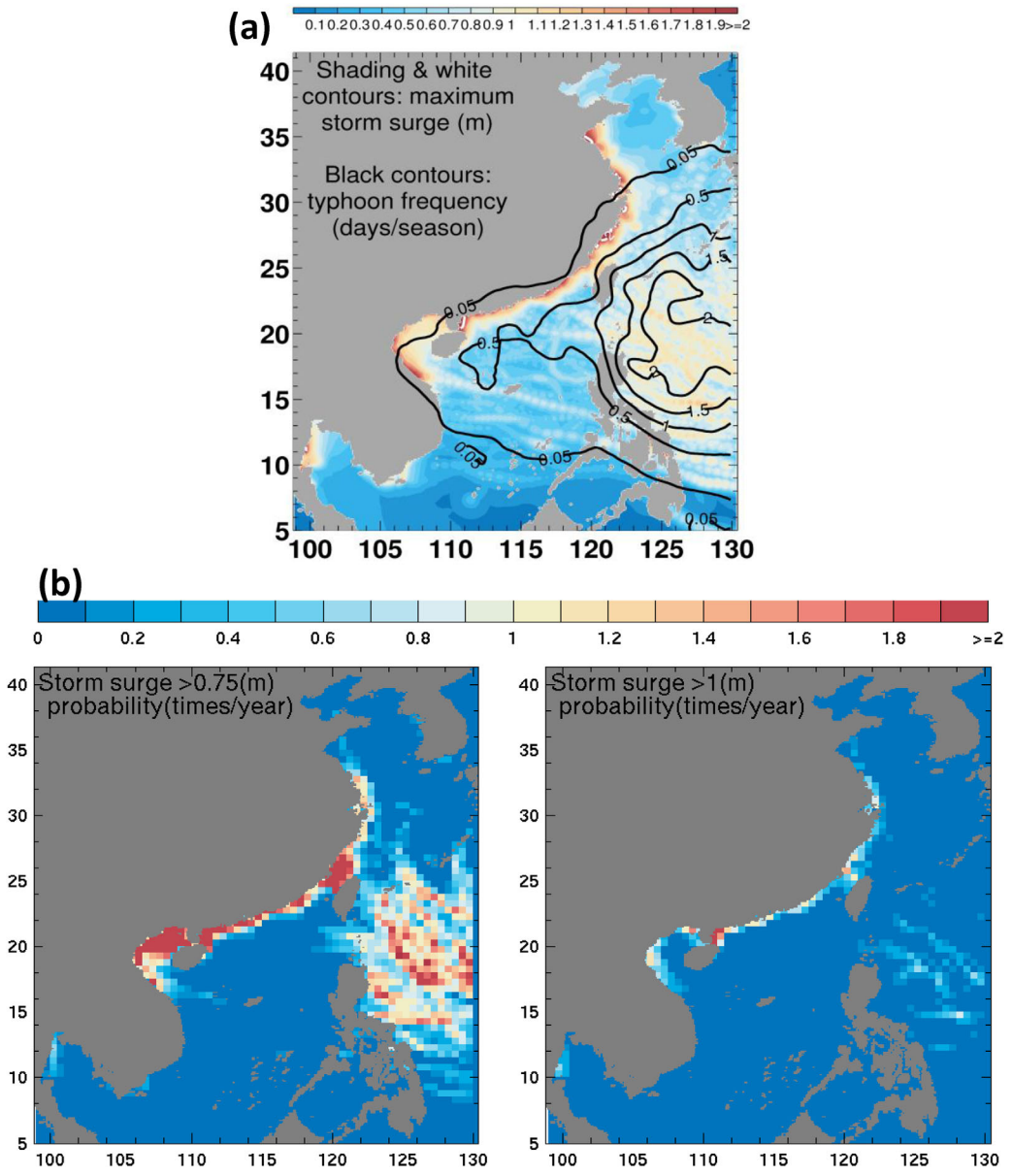

Figure 2. (a) Model maximum storm surge (m; shading and white contour = 2 m) during the typhoon season (June–November) in the western North Pacific from 1950 to 2013. Black contours show typhoon frequency $f_{tc}(\mathbf{x})$: "1" indicates location where, on average from 1950 to 2013, the grid experiences 1 day of typhoon-strength wind (maximum sustained wind speeds > 33 m s^{-1}) per season. (b) Averaged number per season of storm surge exceeding (left) 0.75 m and (right) 1 m; scale is such that red is > 2 times per season.

Western Pacific typhoons are known to display interannual and longer variability dependent on ENSO and PDO [*Elsner and Liu*, 2003; *Emanuel*, 2005; *Camargo et al.*, 2007; *Chan*, 2008; *Wang and Liu*, 2015]. To examine how ENSO and PDO affect the storm surge trends, we remove their linear regressions with $<\eta_{Smax}>$, $<\theta_{Smax}>$, and $<t_{SS>0.7m}>$ (supporting information Figure S3) and recalculate the trends (Table 1). The connections between all three storm surge variables with ENSO and/or PDO are weak and statistically insignificant, with *p*-values of the regressions varying from $p = 0.53$ to 0.93. For $<\eta_{Smax}>$ and $<t_{SS>0.7m}>$, Figures 3a and 3c are only slightly changed if ENSO and PDO influences are removed (Table 1). For $<\theta_{Smax}>$, it has an overall negative correlation with PDO (though with little confidence $p = 0.53$), and therefore does contribute to the corresponding trend shown in Figure 3b. Therefore, when the influence of PDO is removed, the overall effect is to slightly decrease the 1982–2013 poleward trend (Figure 3b), from 0.92°/decade to 0.82°/decade. At the same time, the significance degraded from $p = 0.10$ to $p = 0.14$. These results appear

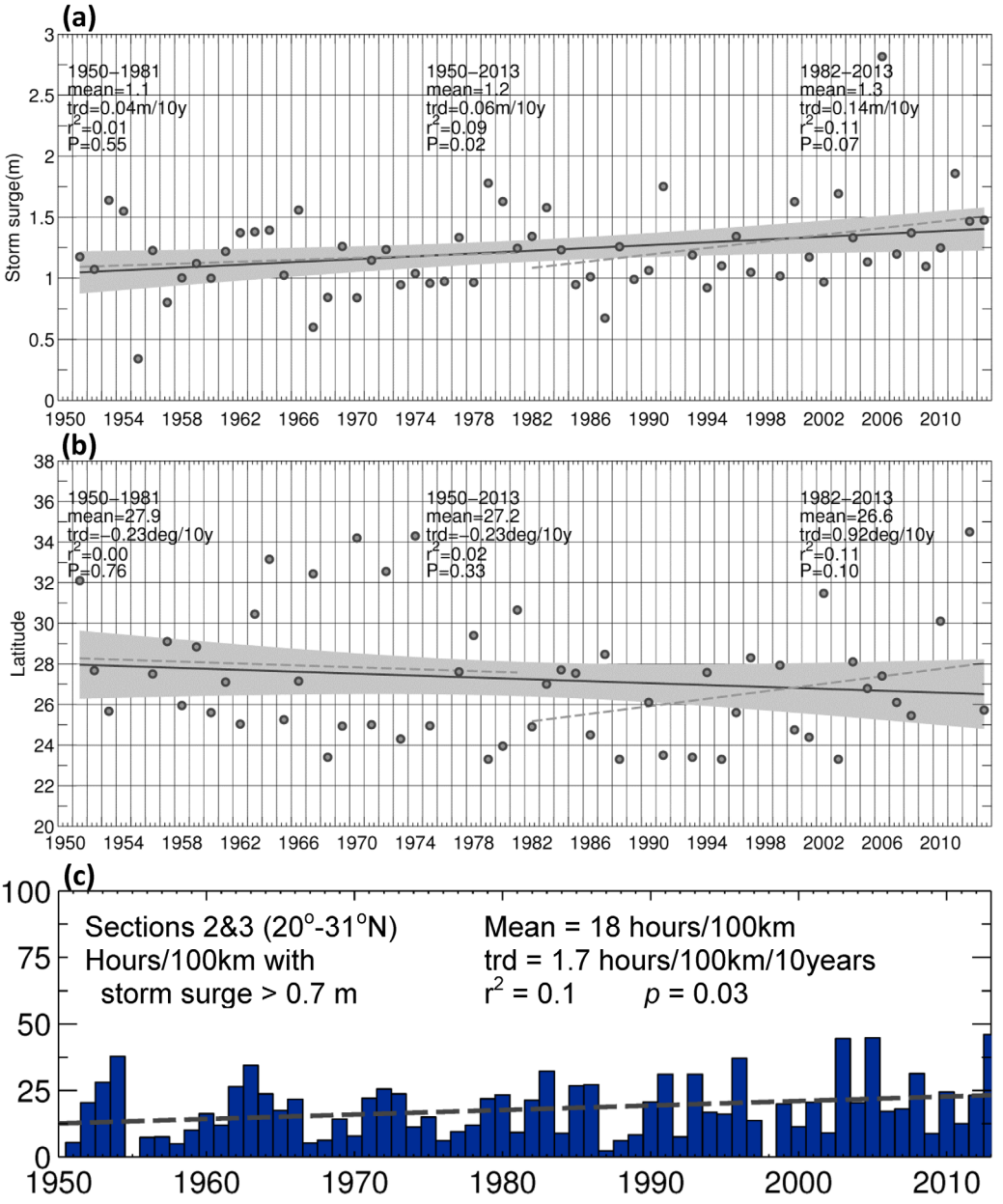

Figure 3. Seasonally mean (i.e., mean for typhoon months from June through November) of (a) monthly maximum storm surge (SS) $<\eta_{Smax}>$ and (b) their corresponding mean latitudes $<\theta_{Smax}>$ along the East Asian coast. Solid and dashed lines show regressions for the whole period 1950–2013 (solid), and separately for 1950–1981 and 1982–2013 periods (dashed). Legends display the period, mean (in unit of *m* or *degree latitude*), trend (trd; in unit of *m* or *degree latitude* per 10 *years*), and the r^2 and *p* values. (c) Number of *hours* per 100 km coastline from 20° to 31°N (along-coastal sections 2 and 3 in Figure 1d) when storm surge exceeds 0.7 m: $t_{SS>0.7m}$. Legends in top right display mean, trend (trd), r^2 and *p* values. All values are calculated for the ensemble mean of experiments using the four different wind products (see Method).

to be consistent with *Kossin et al.* [2014], who concluded when discussing the latitude of TC lifetime-maximum intensity (LMI) that it is ". . .unlikely that natural ENSO variability has a role in the observed multi-decadal poleward migration of LMI. . ." The authors also stated that: ". . .The potential for contributions from natural variability occurring on decadal or longer timescales still exists, but quantifying this is difficult using relatively short observation records." As our time series is also relatively short, the statement is probably also true in our case. On the other hand, it is inappropriate to draw an exact analogy, because storm surge response involves added complexity of coastal shelf dynamics (e.g., trapped waves) that are not a simple function of location of TC-landing.

Table 1. Trends and *p*-Values of $<\eta_{Smax}>$, $<\theta_{Smax}>$ and $t_{SS>0.7m}$ Calculated From the Total (i.e., Figure 3) as Well as the Time Series From Which ENSO and PDO Are Removed

	Total	ENSO Removed	PDO Removed
$<\eta_{Smax}>$ m/decade	0.14	0.14	0.13
p	0.07	0.07	0.08
$<\theta_{Smax}>$ deg/decade	0.92	0.95	0.82
p	0.10	0.08	0.14
$t_{SS>0.7m}$ (hours/100 km/decade)	1.7	1.7	1.6
p	0.03	0.03	0.03

3.2. Observed Storm Surge Trends

Maximum storm surge at individual tide-gauge stations is calculated and then averaged over each typhoon season to yield $<\eta_{TGSmax}>$. Observed trends for $<\eta_{TGSmax}>$ generally show rising trends which range from low 0.03–0.04 m per decade for stations around Taiwan, to moderate 0.07–0.11 m per decade at the northern China stations, and strong 0.14–0.17 m per decade at the southern (Zhapo and Haikou) and middle (Kanmen) stations (supporting information Figures S1–S2 and Table S2).

An analysis following Figure 3 (for model) yielded poor statistics, since tide-gauge stations are too few and too sparsely spaced to determine trends of storm surge maxima $<\eta_{Smax}>$. We use instead the 95 and 99 centiles to characterize storm surge extremes from 1975 to 1997 (Figure 4a). Both show rising trends of 0.12 and 0.15 m per decade from 1982 to 1997, significant at the 97% and 93% confidence levels, respectively. Note that the analysis requires concurrent measurements along the China coast, which limits the time period from 1975 to 1997. In agreement with the modeled trend (Figure 3a), the observed trends during the earlier period before 1982, albeit shorter, are insignificant. The tide-gauge stations are also too sparsely

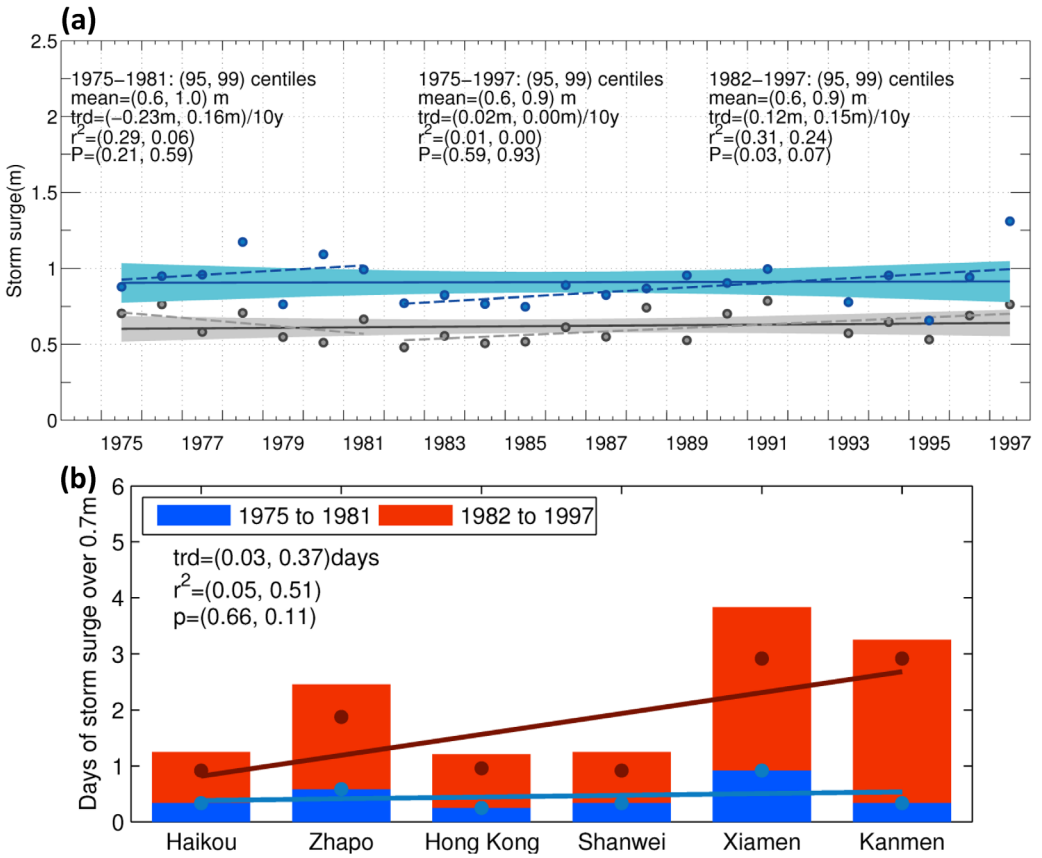

Figure 4. (a) The 95 (grey) and 99 (blue) centiles of observed storm surge at tide-gauge stations that have at least 23 years of concurrent measurements from 1975 to 1997. Solid and dashed lines show regressions for the whole period 1975–1997 (solid), and separately for 1975–1981 and 1982–1997 periods (dashed). Legends display the period, mean (in unit of *m*), trend (trd; in unit of *m* per 10 *years*), and the r^2 and *p* values. (b) Days of storm surge > 0.7 m at the indicated tide-gauge stations from south to north along the China coast —the stations are all within the along-coast sections 2 and 3 shown in Figure 1d—for the indicated two separate periods: 1975–1981 (blue bars and dots) and 1982–1997 (red bars and dots).The trends (trd in days per station, r^2 and *p* values are displayed in the top left).

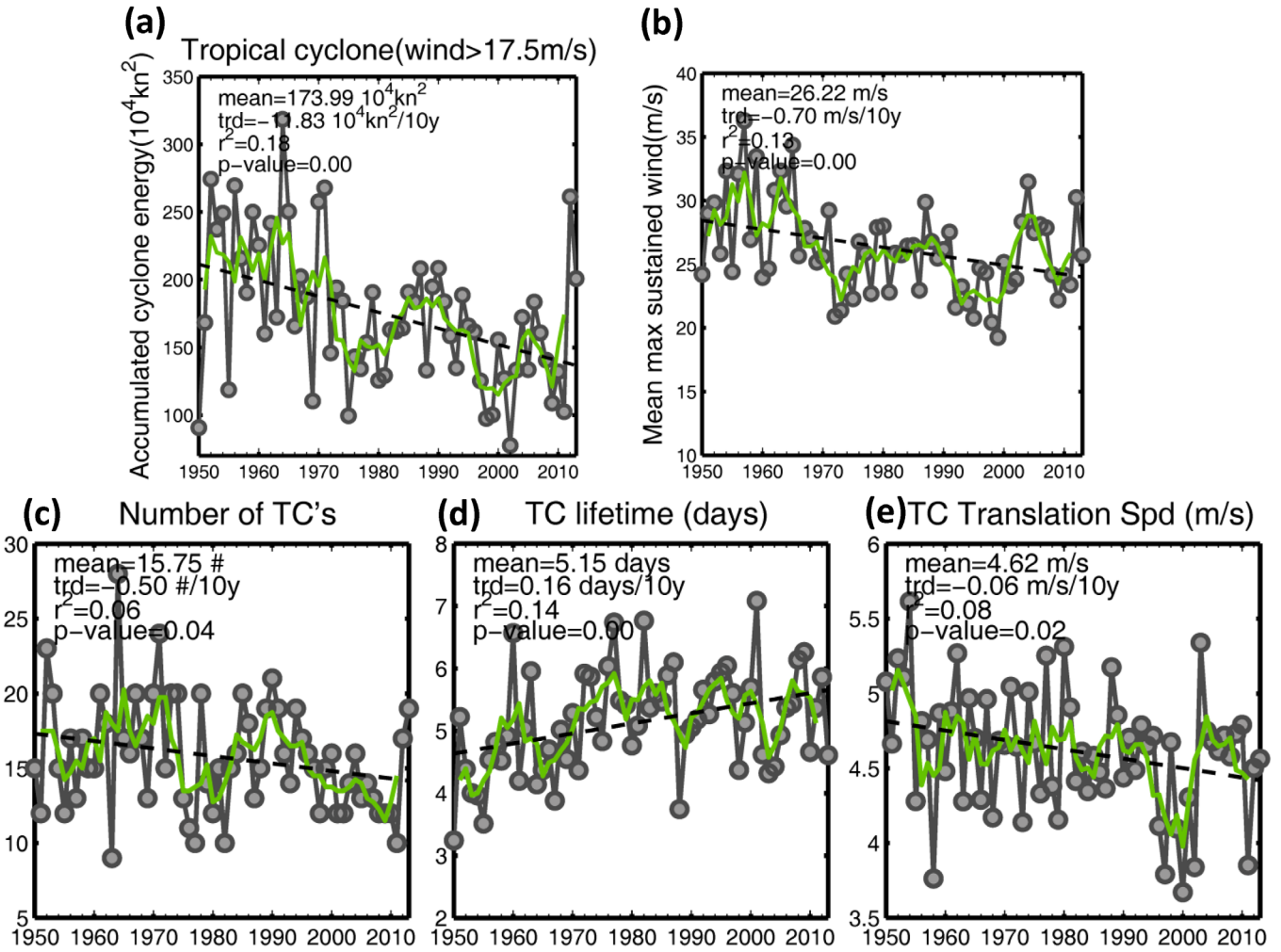

Figure 5. TC statistics from 1950 to 2013: (a) annual-mean accumulated cyclone energy (ACE), (b) annual-mean maximum sustained wind speed, (c) TC number, (d) annual-mean TC lifetime, and (e) annual-mean translation speed, in the indicated units. In each plot, thick green line shows the 5 year running mean, and legends display the total mean, trend (trd), and the corresponding r^2 and p values.

spaced to define a meaningful $<\theta_{Smax}>$. Instead, we examine if the rising trends are accompanied by a poleward shift of storm surges by comparing the number of days for surges exceeding 0.7 m for stations from south to north along the China coast, for two periods: 1975–1981 and 1982–1997 (Figure 4b). The calculation was done between stations Haikou and Kanmen where the typhoon frequency $f_{tc}(\boldsymbol{x})$ is approximately the same (Figure 2a; so that differences in the number of storm surge days are not because of $f_{tc}(\boldsymbol{x})$). For the earlier period from 1975 to 1981, the change in storm surge days from the southern to northern stations is small and insignificant ($p = 0.66$). For the later period from 1982 to 1997; however, there is an overall increase in storm surge days of about 1.85 days from south to north, significant at the 89% confidence level.

3.3. Effects of Large-Scale Sea-Level Rise

The model's rising trends of $<\eta_{Smax}>$ of 0.06–0.14 m per decade (Figure 3a and Table 1) are weaker than the observed trends of 0.07–0.17 m per decade for the individual stations (supporting information Figure S2 and Table S2). In addition to the rising trend in storm surge, the observation also includes a large-scale sea-level rise which is not accounted for in the model, and which in the western North Pacific Ocean has been significant in recent decades [*Merrifield*, 2011]. Estimates of large-scale sea-level trend using altimetry data yield a rise of 0.02–0.04 m per decade over the East Asian continental shelves [*Merrifield*, 2011; *Merrifield et al*., 2012]. These trends agree very well with the independent estimates calculated using long-term sea level observations from the Permanent Service for Mean Sea Level (PSMSL; http://www.psmsl.org/) data set at five stations (Dalian, Lusi, Kanmen, Hong Kong, and Zhapo) along the coast of China (supporting

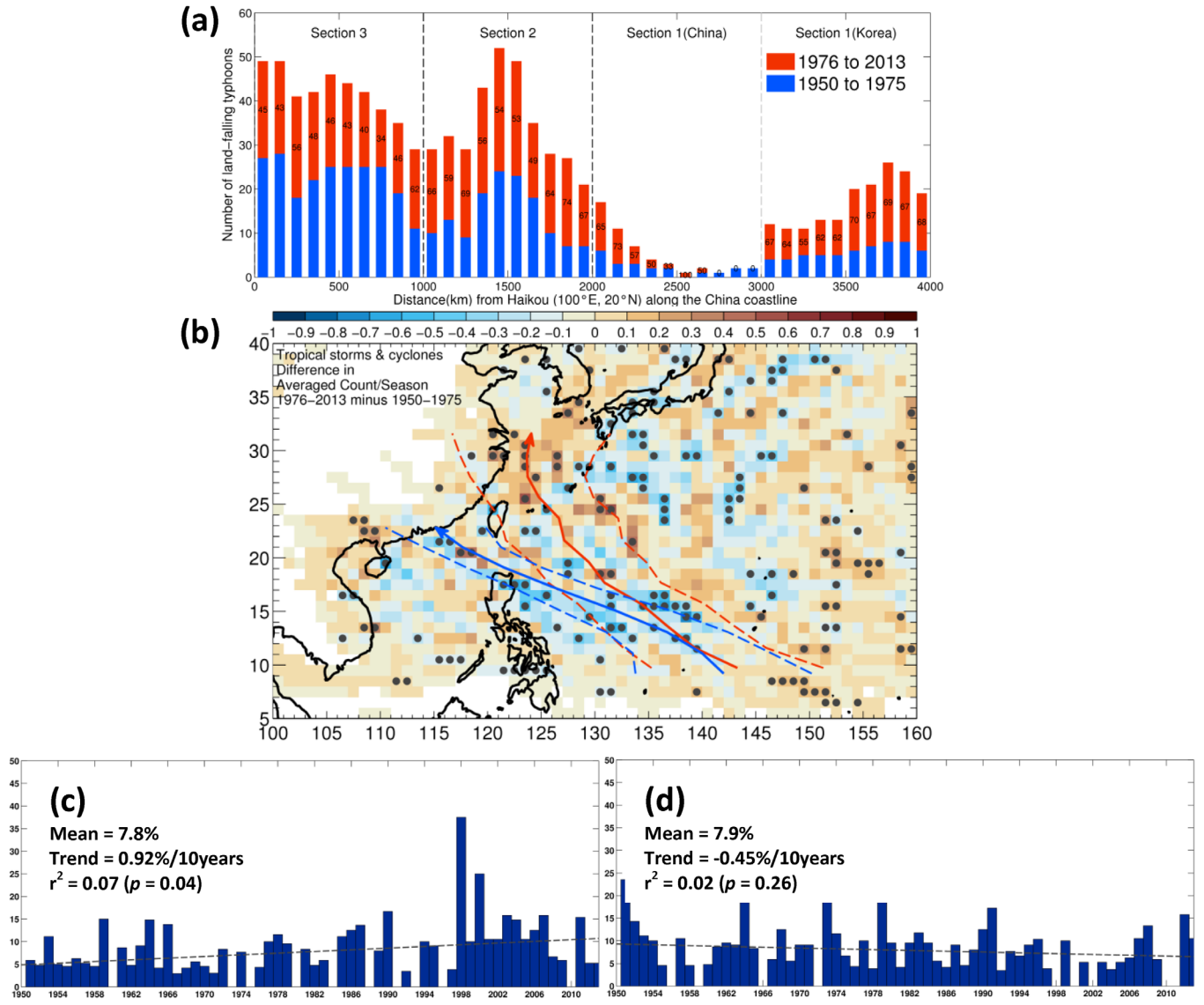

Figure 6. (a) Number of land-falling typhoons as a function of distance in *km* measured from Haikou (110°E, 20°N) along the China coastline shown for two periods: 1950–1975 (blue bars) and 1976–2013 (red bars). Year 1976 is chosen because the total number of typhoons decreases from 1950 to 2013 and 1976 is the break-even point when the numbers before and after are equal. Vertical dashed lines separate the along-coast sections 3 (south), 2 (middle), and 1 (north) (see Figure 1d for section locations). Numbers on red bars are percentages from 1976 to 2013, showing that the number of land-falling typhoons has increased in the later period for the more northern sections. (b) Difference in the average number of TCs per 1° × 1° grid (color, with dots where the difference is significant at the 95% confidence level) between the 2 periods: 1976–2013 minus 1950–1975. Solid red and blue lines show mean tracks over East China Sea and northern South China Sea with dashed lines indicating the 95% confidence envelopes. (c) and (d) are the corresponding yearly numbers of TCs (histograms) for the red and blue tracks, expressed as percentages of the total TCs originating in the North Pacific Ocean from 130°E to 180°E.

information Figure S4). These long-term, rising trends of large-scale sea-level account very well the difference between the modeled and observed storm-surge trends.

4. Discussions

4.1. Causes of Increasing Trend of Storm Surges and Their Poleward Shift

The rising trends of storm surge may be caused by an increase in TC intensity or number, or both. However, both quantities have decreasing trends (Figures 5b and 5c) in the western North Pacific west of 130°E, so has their corresponding accumulated cyclone energy (ACE; Figure 5a). On the other hand, TC lifetime has increased (Figure 5d), caused by a decrease in the TC translation speed (Figure 5e). With slower storms, the time which they influence the coast lengthens, which then increases the number of surge days (e.g.,

$t_{SS>0.7\ m}$, Figure 3c). A slower-moving storm also would tend to force more extreme surges, since the along-coast wind component of the approaching storm forces sea-level setup that to the first order of approximation linearly increases with time [*Gill*, 1982]. The rising trends of both the storm surge extremes and the number of surge days can therefore be explained by the observed trends of longer-lasting and slower-moving TCs from 1950 to 2013. A potential difficulty in the above interpretations is that the quality of best-track data, in particular the TC intensity, is less reliable prior to ~1980 [*Kossin et al*., 2013]. On the other hand, an otherwise increasing trend of TC intensity is not inconsistent with the rising trends of storm surge (Figure 3a) and, as discussed below, our results for longer-lasting storms with slower translation speeds in the western North Pacific are consistent with other studies using data from more recent periods.

The northward shift of more storm surge after 1982 along the coast of China (Figure 3b) can be explained by a general tendency for TCs to make land-falls at more poleward locations along the coast of China in recent decades. To show this, we compare the number of land-falling TCs along the coast before and after 1976 (Figure 6a), chosen because it is the break-even year between 1950 and 2013 when the number before and after is equal (Figure 5c). The number of land-falling TCs has increased (decreased) north (south) of 23°N for the period 1976–2013 compared to the earlier period 1950–1975. Along the southern China coast (along-coast distance $s = 0$ to 1000 km in Figure 6a) for example, the number of land-falling TCs has dropped below 50% after 1976, but at locations further north ($s > 1000$ km) the number has increased to above 50%. In western North Pacific, the difference in the average number of TCs per $1° \times 1°$ grid between the two periods: 1976–2013 minus 1950–1975, is significantly positive north of Taiwan over East China Sea, while east of Luzon and over South China Sea the average number tends to be negative or neutral (Figure 6b). The TC-histogram for the northern track which passes over East China Sea shows a significant increasing trend (Figure 6c) at the 96% confidence level, while that along the southern track into South China Sea has a decreasing trend with low (74%) confidence level (Figure 6d).

4.2. Connection With Climate Warming

The slowdown of TC translation and the tendency for TC tracks to more readily recurve in recent decades are closely related to the weakening of the easterly steering flow over the tropical and subtropical western North Pacific (5°N–30°N), which in turn have been connected to climate warming [*Wu et al*., 2005; *Tu et al*., 2009; *Chu et al*., 2012]. Coupled large-scale wind and SST as well as coupled air-sea processes for individual TCs can potentially influence the shift in location of TC genesis and tracks [*Chan and Liu*, 2004; *Wu et al*., 2005; *Li et al*., 2010; *Chu et al*., 2012; *Ogata et al*., 2015; *Wang and Liu*, 2015; *Wang et al*., 2015]. *Zhou et al*. [2009] has suggested that the western Pacific subtropical high has extended more westward since the late 1970s, due to warming of the Indian Ocean and western Pacific. High-resolution model projection (2075–2099) by *Murakami et al*. [2011] suggests that the steering flow is likely to further weaken as the climate warms. The weakening is generally consistent with climate model simulations which show that, as the planet warms, the increase in the vigor of the hydrological cycle is slower than the Clausius-Clapeyron relation would indicate [*Boer*, 1993], suggesting a decrease in the strength of large-scale circulations like the Walker and Hadley circulations [*Held and Soden*, 2006], and an increase in sea-level pressure over the maritime continent [*Vecchi et al*., 2006]. Moreover, the location of TC maximum intensity has shifted poleward in recent decades [*Kossin et al*., 2014] particularly in the western North Pacific [*Kossin et al.,* 2016], which can further favor northward shift of storm surges. The present study shows that such climate warming-related changes can have nonnegligible effects on storm surge distribution and intensity, which policy planners need to take into account in order to balance economical advances associated with coastal developments with the well-being of population.

Acknowledgements
We thank the reviewers for providing useful comments. All the data used in this manuscript are available by emailing the corresponding author L.-Y. Oey at lyo@princeton.edu. Y.-C. Lin helped with some of the analyses and graphics.

References

Aon Benfield (2013), Annual global climate and catastrophe report, impact forecasting: 2013. Report published by Aon Benfield, a division of Aon plc., http://www.aon.com/reinsurance/. [Available at http://thoughtleadership.aonbenfield.com/Documents/20140113_ab_if_annual_climate_catastrophe_report.pdf.]

Aschariyapotha, N., P. Wongwises, U. W. Humphries, and S. Wongwises (2011), Study of storm surge due to Typhoon Linda (1997) in the Gulf of Thailand using a three dimensional ocean model, *Appl. Math. Comput.*, *217*(21), 8640–8654.

Balmaseda, M. A., K. E. Trenberth, and E. Kallen (2013), Distinctive climate signals in reanalysis of global ocean heat content, *Geophys. Res. Lett.*, *40*, 1754–1759, doi:10.1002/grl.50382.

Bender, M. A., T. R. Knuston, R. E. Tuleya, J. J. Sirutis, G. A. Vecchi, S. T. Garner, and I. M. Held (2010), Modeled impact of anthropogenic warming of the frequency of intense Atlantic hurricanes, *Science*, *327*, 454–458.

Boer, G. J. (1993), Climate change and the regulation of the surface moisture and energy budgets, *Clim. Dyn.*, *8*, 225–239.

Bromirski, P. D., and J. P. Kossin (2008), Increasing hurricane wave power along the U.S. Atlantic and Gulf coasts, *J. Geophys. Res.*, *113*, C07012, doi:10.1029/2007JC004706.
Camargo, S.J., K. Emanuel, and A.H. Sobel (2007), Use of a genesis potential index to diagnose ENSO effects on tropical cyclone genesis, *J. Clim.*, *20*, 4819–4834.
Cartwright, D. E. (1978), Oceanic tides, *Int. Hydrogr. Rev.*, *55*(2), 35–84.
Chan, J. C. L. (2005), The physics of tropical cyclone motion, *Annu. Rev. Fluid Mech.*, *37*, 99–128.
Chan, J. C. L. (2008), Decadal variations of intense typhoon occurrence in the western North Pacific, *Proc. R. Soc. A*, *464*, 249–272.
Chan, J. C. L., and K. S. Liu (2004), Global warming and western North Pacific typhoon activity from an observational perspective, *J. Clim.*, *17*, 4590–4602.
Chen, C., and Z. Qin (1985), Numerical simulation of typhoon surges along the east coast of Zhejiang and Jiangsu Provinces, *Adv. Atmos. Sci.*, *2*, 8–19.
Chow, V. T. (1959), *Open-Channel Hydraulics*, 680 pp., McGraw-Hill, N. Y.
Chu, P. S., J.-H. Kim, and Y.-R. Chen (2012), Have steering flows in the western North Pacific and the South China Sea changed over the last 50 years?, *Geophys. Res. Lett.*, *39*, L10704, doi:10.1029/2012GL051709.
Cummins, P. F., and L-Y. Oey (1997), Simulation of barotropic and baroclinic tides off northern British Columbia, *J. Phys. Oceanogr.*, *27*(5), 762–781.
Deng, Z., F. Zhang, L. Kang, X. Jiang, J. Jin, and W. Wang (2014), East China Sea Storm surge modeling and visualization system: The typhoon Soulik Case, *Sci. World J.*, Article ID 626421, 7 pp., doi:10.1155/2014/626421.
Ding, Y., and L. Ding (2014), A numerical simulation of extratropical storm surge and hydrodynamic response in the Bohai Sea, *Disc. Dyn. Nat. Soc.*, Article ID 282085, 8 pp., doi:10.1155/2014/282085.
Elsner, J. B., and K.-B. Liu (2003), Examining the ENSO-Typhoon hypothesis, *Clim. Res.*, *25*, 43–54.
Emanuel, K. A. (2005), Increasing destructiveness of tropical cyclones over the past 30 years, *Nature*, *436*(7051), 686–688.
Emanuel, K. A. (2013), Downscaling CMIP5 climate models shows increased tropical cyclone activity 30 over the 21st century, *Proc. Natl. Acad. Sci. U. S. A.*, *110*(30), 12,219–12,224, doi:10.1073/pnas.1301293110.
Feng, X., and M. N. Tsimplis (2014), Sea level extremes at the coasts of China, *J. Geophys. Res. Oceans*, *119*, 1593–1608, doi:10.1002/2013JC009607.
Gill, A. E. (1982), *Atmosphere-Ocean Dynamics*, 662 pp., Academic Press, N. Y.
Goddard, P. B. et al. (2015), An extreme event of sea-level rise along the northeast coast of North America in 2009-2010, *Nat. Commun.*, *6*, 6346, doi:10.1038/ncomms7346.
Gray, W. M. (1984), Atlantic seasonal hurricane frequency. Part I: El Nino and 30 mb quasi-biennial oscillation influences, *Mon. Weather Rev.*, *112*, 1649–1668.
Grinsted, A., J. C. Moore, and S. Jevrejeva (2012), A homogeneous record of Atlantic hurricane surge threat since 1923, *Proc. Natl. Acad. Sci. U. S. A.*, *109*(48), 19,601–19,605.
Grinsted, A., J. C. Moore, and S. Jevrejeva (2013), Projected Atlantic hurricane surge threat from rising temperatures, *Proc. Natl. Acad. Sci. U. S. A.*, *110*(14), 5369–5373.
Han, M., J. Hou, and L. Wu (1995), Potential impacts of sea-level rise on China's coastal environment and cities: A national assessment, *J. Coastal Res.*, *14*, 79–95.
Hansen, J., R. Ruedy, M. Sato, and K. Lo (2010), Global surface temperature change, *Rev. Geophys.*, *48*, RG4004, doi:10.1029/2010RG000345.
Held, I. M., and B. J. Soden (2006), Robust responses of the hydrological cycle to global warming, *J. Clim.*, *19*, 5686–5699.
Ho, C.-H., J.-J. Baik, J.-H. Kim, D.-Y. Gong, and C. H. Sui (2004), Interdecadal changes in summertime typhoon tracks, *J. Clim.*, *17*, 1767–1776.
Holland, G. J. (1980), Analytic model of the wind in hurricanes, *Mon. Weather Rev.*, *108*, 1212–1218.
Holland, G. J. (1983), Tropical cyclone motion: Environmental interaction plus a beta effect, *J. Atmos. Sci.*, *40*, 328–342.
IPCC (2013), *Climate Change 2013: The Physical Science Basis. Contribution of Working Group I to the Fifth Assessment Report of the Intergovernmental Panel on Climate Change*, edited by T. F. Stocker et al., 1535 pp., Cambridge Univ. Press, Cambridge, U. K.
Knapp, K. R., M. C. Kruk, D. H. Levinson, H. J. Diamond, and C. J. Neumann (2010), The International Best Track Archive for Climate Stewardship (IBTrACS): Unifying tropical cyclone best track data, *Bull. Am. Meteorol. Soc.*, *91*, 363–376.
Knutson, T. R., et al. (2010), Tropical cyclones and climate change, *Nat. Geosci.*, *3*, 157–163.
Knutson, T. R., et al. (2013), Dynamical downscaling projections of 21st century Atlantic hurricane activity: CMIP3 and CMIP5 model-based scenario, *J. Clim.*, *26*, 6591–6617.
Knutson, T. R., et al. (2015), Global projections of intense tropical cyclone activity for the late 21st century from dynamical downscaling of CMIP5/RCP4.5 scenarios, *J. Clim.*, *28*, 7203–7224.
Kossin, J. P., T. L. Olander, and K. R. Knapp (2013), Trend Analysis with a New Global Record of Tropical Cyclone Intensity, *J. Clim.*, *26*, 9960–9976.
Kossin, J. P., K. A. Emanuel, and G. A. Vecchi (2014), The poleward migration of the location of tropical cyclone maximum intensity, *Nature*, *509*, 349–352.
Kossin, J., K. Emanuel, and S. Camargo (2016), Past and Projected Changes in Western North Pacific Tropical Cyclone Exposure, *J. Clim.*, doi:10.1175/JCLID-16-0076.1, in press.
Lefevre, F., C. Le Provost, and F. H. Lyard (2000), How can we improve a global ocean tide model at a regional scale? A test on the Yellow Sea and the East China Sea, *J. Geophys. Res.*, *105*, 8707–8725, doi:10.1029/1999JC900281.
Levermann, A., A. Griesel, M. Hofmann, M. Montoya, and S. Rahmstorf (2005), Dynamic sea level changes following changes in the thermohaline circulation, *Clim. Dyn.*, *24*, 347–354.
Li, H.-W., C.-H. Tsai, and Y.-T. Lo (2009), Numerical simulation of typhoon surges along the coast of Taiwan, *Nat. Hazards*, *50*, 413–431.
Li, T., M. Kwon, M. Zhao, J.-S. Kug, J.-J. Luo, and W. Yu (2010), Global warming shifts Pacific tropical cyclone location, *Geophys. Res. Lett.*, *37*, L21804, doi:10.1029/2010GL045124.
Lin, I. I., G. J. Goni, J. A. Knaff, C. Forbes, and M. M. Ali (2013), Ocean heat content for tropical cyclone intensity forecasting and its impact on storm surge, *Nat. Hazards*, *66*, 1481–1500.
Lin, N., et al. (2012), Physically based assessment of hurricane surge threat under climate change, *Nat. Clim. Change*, *2*, 462–467.
Marcos, M., et al. (2015), Long-term variations in global sea level extremes, *J. Geophys. Res. Oceans*, *120*, 8115–8134, doi:10.1002/2015JC011173.
Mellor, G. L. (2004), *Users Guide for a Three-dimensional, Primitive Equation, Numerical Ocean Model (June 2004 Version)*, *Prog. Atmos. Ocean*, 56 pp., *Sci.*, Princeton Univ., Princeton, N. J.
Merrifield, M. A. (2011), A shift in western tropical Pacific sea level trends during the 1990s, *J. Clim.*, *24*, 4126–4138.

Merrifield, M. A., P. R. Thompson, and M. Lander (2012), Multidecadal sea level anomalies and trends in the western tropical Pacific, *Geophys. Res. Lett.*, *39*, L13602, doi:10.1029/2012GL052032.
Mori, N., M. Kato, S. Kim, H. Mase, Y. Shibutani, T. Takemi, K. Tsuboki, and T. Yasuda (2014), Local amplification of storm surge by Super Typhoon Haiyan in Leyte Gulf, *Geophys. Res. Lett.*, *41*, 5106–5116, doi:10.1002/2014GL060689.
Murakami, H., B. Wang, and A. Kitoh (2011), Future change of western North Pacific typhoons: Projections by a 20-km-mesh global atmospheric model, *J. Clim.*, *24*, 1154–1169, doi:10.1175/2010JCLI3723.1.
Needham, H. F., B. D. Keim, and D. Sathiaraj (2015), A review of tropical cyclone-generated storm surges: Global data sources, observations, and impacts, *Rev. Geophys.*, *53*, 545–591, doi:10.1002/2014RG000477.
Nitta T., and S. Yamada (1989), Recent warming of recent sea surface temperature and its relation to northern hemisphere circulation, *J. Meteorol. Soc. Jpn.*, *67*, 375–383.
Oey, L.-Y. (2005), A wetting and drying scheme for POM, *Ocean Modell.*, *9*, 133–150.
Oey, L.-Y. (2006), An OGCM with movable land-sea boundaries, *Ocean Modell.*, *13*, 176–195.
Oey, L.-Y., and P. Chen (1992), A model simulation of circulation in the Northeast Atlantic shelves and seas, *J. Geophys. Res.*, *97*, 20,087–20,115, doi:10.1029/92JC01990.
Oey, L-Y., G. L Mellor, and R. I. Hires (1985), Tidal modeling of the Hudson-Raritan estuary, *Estuarine Coastal Shelf Sci.*, *20*, 511–527.
Oey, L.-Y., T. Ezer, C. Hu, and F. Muller-Karger (2007), Baroclinic tidal flows and inundation processes in Cook Inlet, Alaska: numerical modeling and satellite observations, *Ocean Dyna.*, *57*, 205–221.
Oey, L, Y.-L. Chang, Y.-C. Lin, M.-C. Chang, F.-H. Xu, and H.-F. Lu (2013), ATOP: Advanced Taiwan Ocean Prediction System based on the mpiPOM. Part 1: Model descriptions, analyses and results, *Terr. Atmos. Ocean. Sci.*, *24*(1), 137–158, doi:10.3319/TAO.2012.09.12.01(Oc).
Oey, L.-Y., Y.-L. Chang, Y.-C. Lin, M.-C. Chang, S. Varlamov, and Y. Miyazawa (2014), Cross flows in the Taiwan Strait in winter, *J. Phys. Oceanogr.*, *44*, 801–817.
Ogata, T., R. Mizuta, Y. Adachi, H. Murakami, and T. Ose (2015), Effect of air-sea coupling on the frequency distribution of intense tropical cyclones over the northwestern Pacific, *Geophys. Res. Lett.*, *42*, 10,415–10,421, doi:10.1002/2015GL066774.
Pawlowicz, R., B. Beardsley, and S. Lentz (2002), Classical tidal harmonic analysis including error estimates in MATLAB using T_TIDE, *Comp. and Geos.*, *28*, 929–937.
Peduzzi, P., B. Chatenoux, H. Dao, A. De Bono, C. Herold, J. Kossin, F. Mouton, and O. Nordbeck (2012), Global trends in tropical cyclone risk, *Nat. Clim. Change*, *2*, 289–294.
Powell, M. D., P. J. Vickery, and T. A. Reinhold (2003), Reduced drag for high wind speeds in TCs, *Nature*, *422*, 279–283.
Rayner, N. A., P. Brohan, D. E. Parker, C. K. Folland, J. J. Kennedy, M. Vanicek, T. J. Ansell, and S. F. B. Tett (2006), Improved analyses of changes and uncertainties in sea-surface temperature measured in-situ since the mid-nineteenth century, *J. Clim.*, *19*, 446–469.
Sauvaget, P., E. David, and C. G. Soares (2000), Modeling tidal currents on the coast of Portugal, *Coastal Eng.*, *40*, 393–409.
Sun, J., and L.-Y. Oey (2015), The influence of the ocean on Typhoon Nuri (2008), *Mon. Weather Rev.*, *143*, 4493–4513, doi:10.1175/MWR-D-15- 0029.1.7/15.
Sun, J., L.-Y. Oey, R. Chang, F. Xu, and S. M. Huang (2015), Ocean response to typhoon Nuri (2008) in western Pacific and South China Sea, *Ocean Dyn.*, *65*, 735–749, doi:10.1007/s10236-015-0823-0.
Trenberth, K. E. (1990), Recent observed interdecadal climate changes in the northern hemisphere, *Bull. Am. Meteorol. Soc.*, *71*, 988–993.
Trenberth, K. E., et al. (2007), Observations: Surface and atmospheric climate change, in *Climate Change 2007. The Physical Science Basis*, edited by S. Solomon et al., pp. 235–336, Cambridge Univ. Press, Cambridge, U. K.
Tu, J.-Y., C. Chou, and P.-S. Chu (2009), The abrupt shift of typhoon activity in the vicinity of Taiwan and its association with western North Pacific–East Asian climate change, *J. Clim.*, *22*, 3617–3628, doi:10.1175/2009JCLI2411.1.
Vecchi, G. A., et al. (2006), Weakening of tropical Pacific atmospheric circulation due to anthropogenic forcing, *Nature*, *441*, 73–76.
Walsh, K. J. E., et al. (2015), Hurricanes and climate: The U.S. CLIVAR Working Group on Hurricanes, *Bull. Am. Meteorol. Soc.*, *96*, 997–1017.
Wang, X., and H. Liu (2015), PDO modulation of ENSO effect on tropical cyclone rapid intensification in the western North Pacific, *Clim. Dyn.*, *46*, 15–28, doi:10.1007/s00382-015−2563-8.
Wang X., C. Wang, L. Zhang, and X. Wang (2015), Multidecadal variability of tropical cyclone rapid intensification in the western North Pacific, *J. Clim.*, *28*, 3806–3820.
Wu, L., B. Wang, and S. Geng (2005), Growing typhoon influence on east Asia, *Geophys. Res. Lett.*, *32*, L18703, doi:10.1029/2005GL022937.
Yin, J. J., M. E. Schlesinger, and R. J. Stouffer (2009), Model projections of rapid sea level rise on the northeast coast of the United States, *Nat. Geosci.*, *2*, 262–266.
Zhou, T., et al. (2009), Why the western Pacific subtropical high has extended westward since the late 1970s, *J. Clim.*, *22*, 2199–2215, doi: 10.1175/2008JCLI2527.1.